Localized Fluctuations of Electrochemical Properties in Porous Electrodes of Lithium-Ion Batteries: Beyond Porous Electrode Theory

Igor Traskunov[a,b,c,*], Arnulf Latz[a,b,c]

[a] *Institute of Engineering Thermodynamics, German Aerospace Center (DLR), Pfaffenwaldring 38-40, 70569 Stuttgart, Germany*
[b] *Helmholtz Institute Ulm for Electrochemical Energy Storage (HIU), Helmholtzstraße 11, 89081 Ulm, Germany*
[c] *University of Ulm, 89069 Ulm , Germany*

Abstract

Porous media with complex microstructures are often used as electrodes in lithium-ion batteries (LIBs) and in the other (electro-)chemical systems with heterogeneous reactions. In the battery context, important aspects of their behavior during charge and discharge can be described by homogenized models based on porous electrode theory (like a widely used DFN model). These models use a number of intuitive assumptions that allow neglecting a detailed microstructure description; these assumptions have been partially confirmed using rigorous mathematical homogenization procedures. Microstructure-resolving simulation results have been published recently that hint to the existence of spatially localized fluctuations of overpotential and concentration in porous electrodes that can not be seen in DFN. Proper account of such fluctuations may be important for the phenomena strongly

*Corresponding author
Email addresses: igor.traskunov@dlr.de (Igor Traskunov), arnulf.latz@dlr.de (Arnulf Latz)

affected by the concentrations and potentials locally (like various aging processes). Here, we present the results of a new mathematical framework utilizing perturbation theory with small parameters that allow accurate standard homogenization of LIBs, but also introduces extensions beyond the standard theory. It will be shown theoretically how the fluctuations in question occur, how to estimate them based on cell characteristics, and to demonstrate the existence of well-defined trends and laws. Numerical simulation results are presented that agree with the main theoretical findings. Current, non-spherical particle shape, particle contacts and OCV slope appear to be the main factors affecting the scale of the local fluctuations. Based on the theory, no physically meaningful homogenization limit exists that sets these fluctuations to zero, which explains why they can be clearly seen in microstructure resolving simulations but not in DFN. The findings presented in this paper are decisive for the development of models extending DFN, preserving its computational robustness and yet fully utilizing all the necessary information about microstructure to capture structure induced local fluctuations.
Keywords: lithium-ion battery, microstructure, homogenization, battery degradation, transport equation analysis

---

1. Introduction

The growing importance of electrochemical energy storage devices spurs scientific research aimed at accurate prediction of their properties and their optimization. They can be effectively understood as multiscale hierarchical systems [1, 2]. To predict the functioning of the most widespread current technology in this domain, lithium-ion batteries (LIBs), one has to take into

account a variety of phenomena starting from the ones on the atomistic scale up to the level of electronic control management systems, all of the levels being important for the understanding of battery capacity, power, life cycle and safety limitations. To achieve computational efficiency and robustness of the description, one has to make use of scale separation to determine a few properly averaged parameters on a lower scale which can be transferred to the next larger scale, discarding a huge amount of fine-scale information. E.g. the exact details of the ion free energy landscape in the electrode resolved on the atomic scale are not needed to describe the averaged transport properties of a porous electrode model.

To effectively utilize active material and improve the power density of the batteries, porous electrodes with very complex, stochastic microstructures are used thereby introducing spatial length scales characterizing features of the electrode microstructure as e.g. thickness, particle scale or scale of sub-structures of particles. As a consequence, in the hierarchical multiscale modeling a natural scale separation emerges: while the battery dynamics on the scale of few nanometers and above can be satisfactorily described by a set of equations for the dynamics of continuum fields (which we will define in our context as "microscopic" models), an electrode on the scale of several particles resembles a homogeneous composite material, in which transport and laws for reactions can be upscaled, neglecting non-essential microscopic details (this will be called below as "macroscopic" scale). All the necessary macroscopic parameters in this context are effective parameters, which do not only depend on material properties but also on geometrical properties of the microstructure. Following the logic of multiscale modeling, they can

be extracted from the corresponding microscopic model. A computational advantage of not resolving small geometrical features is self-evident. In electrochemical engineering, the approaches based on such upscaling ideas can be traced back to the porous electrode theory by Newman and coworkers [3]. They gave rise to a class of models, the basic and widely accepted one being those of Doyle, Fuller and Newman (DFN) [4, 5, 6, 7]. Over the years, the upscaling concept at the model's foundation was supplemented by various ideas, aiming at the incorporation of multiple phenomena in the electrode, like thermal, mechanical deformation, degradation reactions, phase transitions, and so on [8, 9, 10, 11, 12, 13, 14, 15].

To make the multiscale modeling in LIBs consistent, it is desirable to formulate the upscaling rules between the levels as rigorously as possible, so that one can clearly understand how the parameters are defined and transferred between the levels. Despite the simplicity of the ideas at the root of the porous electrode theory, some of the assumptions are not straightforwardly testable and justifiable, and it can make the transition to this model in the context of the hierarchical approach a methodological bottleneck. A body of research started to emerge that addresses the details of microscopic solutions that can not be accurately reproduced with the help of the homogenized porous electrode theory-based models.

Latz and Zausch studied the problem of relation between DFN and the corresponding microscopic transport theory with the help of numerical modeling [2]. In particular, they looked into how accurately the former can reproduce the thermal properties coming from the local distribution of heat spots in the latter. As a byproduct of this analysis, they discovered that the

distribution of overpotential in the electrode obtained from the microscopic simulation is quantitatively and qualitatively different from the one from DFN. Namely, the overpotential exhibits seemingly chaotic strong spatial variation on the microstructure particle scale; at the same time, the running average along the through-plane direction of the electrodes agrees well with the DFN results.

We will refer to this type of cell physical quantity variation on the microstructure-resolving scale as to local fluctuations. In this paper, we aim at developing a theory of such fluctuations. The results of Latz and Zausch hint that they are closely linked to the problem of the relation between the DFN-type cell models and their microstructure-resolving continuous media counterparts, and it can be seen from the following arguments. The formal volume averaging procedure is the main mathematical instrument used to derive the former from the latter. Researchers used homogenization theory, a mathematical framework to describe the upscaling of differential equation problems with scale separation, to prove the correctness of the volume averaging use in the electrochemical modeling, i.e. that deviations from the averaged fields really disappear from the resulting DFN limit [16, 17, 18, 19, 20]. But upon closer inspection, it can be shown that homogenization can not be applied to the lithium mass transport in the active material on the time scales typical for battery dynamics, in contrast to the other processes. In DFN, one uses the effective spherical particle representation to capture these phenomena as an alternative to the exact solution of the mass transport equation in complex geometry. Due to the resulting internal geometric symmetry, an interface variation of any physical quantity on the scale of one particle is always zero.

The pronounced overpotential fluctuations from [2] are exactly this type of fluctuations, and the link between them and the accurate transition between the models is thus established. The fluctuations should be as much noticeable as the deviation of the DFN solution from the microscopic model solution.

At the same time, the representation of the microstructure as a collection of effective spherical particles of finite size is important for the model's validity. It allows DFN to reproduce important cell properties, such as capacity decrease at high C-rates and its connection to the particle size. It would not be so if the ion diffusion in the solid phase was accurately represented by a purely homogenized volume-averaged process since this would imply that particle size as a parameter had to be absent from the homogenized model. To the best of our knowledge, no rigorous mathematical derivation or explanation of the spherical particle approximation has been given.

In the following, we will present a theoretical approach, in which the transition from a microscopic to a macroscopic cell description is closely linked to the local fluctuations. We start with the equations constituting a microstructure-resolving model and then outline how the introduction of a number of approximations will lead to a somewhat simpler model. These approximations constitute a stricter set of conditions than the ones usually employed in the homogenization analysis of porous cell electrodes but are still correct for real microstructures. Through this, we will end up with a media representation as a sum of separate particles, whose dynamics can be evaluated mathematically independently of one another; the representation is very close to the DFN picture but will generalize their model to independent particles of non-spherical shape. We will, in addition, show that the non-

spherical shape is a major cause of the observed overpotential fluctuations. A further linearization approximation of the equations allows us to extract more analytical results about the particle-scale fluctuations and to quantify how far the true microstructure-resolving solution on this level deviates from the idealized spherical geometry.

Importantly, while outlining these steps, we will indicate a number of useful results about the local fluctuation behaviour. To this end, we will closer analyse the equations for the perturbation terms in our ansatz. A part of these equations is identical to the ones that appear in the homogenization procedure, but are usually discarded in the battery literature, aiming at the limit of fully homogenized solution. In the context of the fluctuation theory, the perturbation solutions are important on their own right since they constitute a part of a difference between the microscopic description and DFN and may thus include the local fluctuations. In total, it is not rare that electrodes consist only of about 10-20 particles per electrode's thickness, and the scale separation may not always accurately hold in electrochemical systems, thus making the understanding of the perturbation solutions valuable for the theory.

Our approach allows to identify the parameters of the microstructure and of the cell dynamics that are most critical for determining the local fluctuation dynamics and scale. A number of heuristic rules and approximate formulas can be proposed that allow estimating the scale and the behaviour of the local fluctuations without utilizing computer simulations.

As an important insight, our approach demonstrates that there are local fluctuations which are not small compared to DFN and therefore are part

of the zeroth-order solution in our perturbation theory. Thus we prove, rigorously, that DFN is not an exact limit of microscopic continuous transport models of LIBs. Overall, the approach opens a possibility for developing a class of models that modify DFN while preserving its basic efficiency, yet incorporating the local fluctuations.

The paper is organised as follows. The material is split into two main sections, one for the theory and one for the numerical simulation results. The theoretical section 2 first reviews the microstructure-resolving continuous model that we use as a reference, to which one compares our results, both theoretically and numerically. Here we also outline the homogenization-based DFN counterpart of this model. The next subsections consist of the presentation of our core new results about the transition between the microscopic description and its homogenized approximation together with the new theoretical insights about the local fluctuations derived from them. Section 3 contains numerical tests aiming to illustrate and support the results from section 2. Some additional elements of the theory are also presented here, that are easier to understand directly in the context of the simulation results.

2. Theory

The microscopic model of lithium-ion battery dynamics that we will use in this paper is derived based on the requirements of thermodynamic consistency [21, 2]. This model treats cell as a microstructure whose 3D details are fully resolved. It is the reference system in the context of the current research. Solutions obtained with other models are compared to it. The corresponding

DFN model based on porous electrode theory will also be reviewed.

2.1. Transport model and porous electrode theory

The cell consists of four phases: electrolyte, cathode and anode active material, conductive material and current collector. Electrical double layer is not resolved. Lithium inside the electrolyte phase is given by the concentration c_e and the electrochemical potential ϕ_e and inside the an active material phase by the concentration c_s and the electrical potential Φ_s. The conductive material and current collector contain no lithium ions and their state is discribed only by the potential Φ_s. The system evolution obeys the equations of mass balance and charge neutrality:

$$\begin{aligned} \frac{\partial c_e}{\partial t} &= -\vec{\nabla}\vec{N_e}, & \frac{\partial c_s}{\partial t} &= -\vec{\nabla}\vec{N_s}, \\ 0 &= -\vec{\nabla}\vec{j_e}, & 0 &= -\vec{\nabla}\vec{j_s}, \end{aligned} \tag{1}$$

where each equation is solved in the phase in which the corresponding variables are defined. $\vec{N}_{e,s}$ is the lithium ion flux and $\vec{j}_{e,s}$ is the electric current. The model stipulates their dependence on the system state:

$$\begin{aligned} \vec{j_e} &= -\kappa_e\vec{\nabla}\phi_e - \kappa_e\frac{1-t_+}{F}\frac{\partial\mu_e}{\partial c_e}\vec{\nabla}c_e, \\ \vec{j_s} &= -\sigma_s\vec{\nabla}\Phi_s, \\ \vec{N_e} &= -D_e\vec{\nabla}c_e + \frac{t_+}{F}\vec{j_e}, \\ \vec{N_s} &= -D_s\vec{\nabla}c_s. \end{aligned} \tag{2}$$

κ_e is the electrical conductivity of the electrolyte, σ_s is the electrical conductivity of either the conductive material or the active material, D_i denotes the

lithium ion diffusion coefficient in the phase i, t_+ is the transference number and μ_e is the lithium chemical potential.

To solve the model, one has to add boundary conditions between the phases. For the interfaces between electrolyte and active material phase the normal flux and the normal current are continuous and depend on the rate of intercalation reaction:

$$\begin{aligned} \vec{j_s} \cdot \vec{n}_{se} = \vec{j_e} \cdot \vec{n}_{se} = i_0, \\ \vec{N_s} \cdot \vec{n}_{se} = \vec{N_e} \cdot \vec{n}_{se} = \frac{i_0}{F}. \end{aligned} \tag{3}$$

For the interfaces between electrolyte and conductive material or current collector we set the normal flux and current to zero. The two conditions on the boundary between the active material and conductive material or current collector are: continous electric potential and zero lithium ion normal flux. For the current i_0 one can use different expressions based on the type of the reactions and the interfaces one considers. For the lithium (de-)intercalation from the electrolyte into the anode particle we will employ the symmetric Butler-Volmer formula [2, 22]:

$$i_0 = 2i_{00}\sqrt{c_e c_s (c_s^{max} - c_s)} \sinh\left(\frac{F}{2RT}\eta\right), \tag{4}$$

although this particular choice is not critical for the resultst of the paper. η is the reaction overpotential:

$$\eta = \Phi_s + \frac{1}{F}\mu_s - \phi_e = \Phi_s - U_0 - \phi_e, \tag{5}$$

where we introduced the open circuit potential (OCV) U_0. The expression after the second equal sign is correct if one measures μ_e relative to metallic

lithium. Another type of interface reaction that we will utilize is the lithium intercalation from the electrolyte into the cathode. The reaction current is calculated according to the formula

$$i_0 = 2k \sinh\left(\frac{F}{2RT}\eta\right), \tag{6}$$

This Butler-Volmer modification does not depend on the ion concentration in the cathode and is suitable for half-cell simulations that we ran for this paper. In this setting the ion concentration in the cathode is not tracked to remove a redundant complexity, hence the formula (6).

The model above allows one to study the electrochemical processes on the scale starting from few nanometers, as long as continuous medium assumption is applicable. Its use for numerical simulation of macroscopic cells becomes however computationally very expensive if one resolves fine details of microstructure. As an alternative, the porous electrode theory was developed by Newman and coworkers, which resulted in the Doyle-Fuller-Newman (DFN) model [16, 17, 18, 19]. This ansatz treats porous electrode as macroscopic homogeneous medium. The exact mathematical formulation depends on the underlying microscopic systems and can be found in the referred literature. We will describe and later refer to the variant compatible with the microscopic model from the equations (1, 2, 3). The state variables c_e, ϕ_e and Φ_s are averaged over macroscopic space regions of the electrode (representative control volumes) and the transport equations for these averaged variables are the modified versions of the equations of the microscopic model. For example, the mass balance equation in the electrolyte is

$$\frac{\partial \epsilon c_e}{\partial t} = -\vec{\nabla}\left(-\epsilon D_e^{eff}\vec{\nabla}c_e + \frac{t_+}{F}\vec{j_e}\right) + \frac{1}{F}ai_0. \tag{7}$$

ϵ is the microstructure porosity. a and i_0 are the specific surface area of the active material in the electrode and the intercalation reaction current from the active material into the electrolyte respectively. The source term represents the volume averaging of the ions moving into the electrolyte. The equations imply that the formulas for the fluxes and the currents are identical to (2), but with the effective transport parameters (D_e^{eff},...) on the microscopic scale that are usually not identical to their microscopic counterparts. The use of the averaging procedure for the equations can be justified with different level of mathematical rigour [16, 17, 18, 19, 20].

The only equation that is not subjected to averaging in this model is the mass balance equation for the lithium ion concentration in the active material, and this fact, as we stressed in the introduction, is important for the understanding of the paper results. Diffusion occurs on the length scale of active material particles but the time scale of diffusion in these particles is comparable with transport processes on cell scale. Therefore the diffusion in the particle can not be represented by a process in the homogenized media on macro scale. To incorporate the effects of the diffusion in the active material into the model, the complex spatial distribution of diffusion processes in the ensemble of active particles in the control volume is substituted by one effective spherical particle whose size depends on the porosity and the specific surface area. The spherical symmetry of this representative particle allows reducing the equation to one spatial dimension. The resulting reaction current on the particle surface is substituted into the averaged equations of the type of (7) to make the system closed. We will write down both the microscopic mass balance equation in the active material and its counterpart for the effective

particle in the porous electrode theory with the corresponding boundary conditions for use as a reference below. The former is

$$\begin{aligned} \frac{\partial c_s}{\partial t} &= \vec{\nabla}(D_s \vec{\nabla} c_s), \\ D_s \frac{\partial c_s}{\partial n} &= -\frac{i_0}{F} \text{ on the interface} \end{aligned} \tag{8}$$

and the one-dimensional version for the effective particle is

$$\begin{aligned} \frac{\partial c_s}{\partial t} &= \frac{D_s}{r^2} \frac{\partial}{\partial r} \left(r^2 \frac{\partial c_s}{\partial r} \right), \\ D_s \frac{\partial c_s}{\partial r} &= -\frac{i_0}{F} \text{ at } r = R, \\ D_s \frac{\partial c_s}{\partial r} &= 0 \text{ at } r = 0. \end{aligned} \tag{9}$$

2.2. Origins of the local fluctuations in the electrode

Latz and Zausch [2] made an extensive numerical comparison of a microscopic cell model with the corresponding porous electrode theory model. The model they used is a modified version of the one based on equations (1-3) with additional terms that represent the coupling with temperature gradients and are based on non-equilibrium thermodynamics. The main focus of the comparison was to investigate the differences between thermal behavior predictions of both models, in particular the role of the localized thermal hot spots that are averaged out in the porous electrode theory. It was demonstrated that on the microstructure scale the temperature gradients contribution is negligible, so the results of [2] hold for the model presented above as well. One crucial observation of this numerical study was, that the overpotential exhibits considerable fluctuations around its running average, yet this running average agrees well with the curve obtained from the porous electrode

theory simulation. The latter can not, by definition, capture the localized spatial fluctuations because the theory deals only with the spatially averaged quantities. Yet, the observed local fluctuations of the overpotential can have serious practical as well as theoretical implications for the development of macroscopic cell models. A most relevant implication of fluctuations of the overpotential might be the occurrence of localized side reaction, as e.g. lithium plating, which would not be captured by the macroscopic model. A subtle theoretical consequence follows from the observation that contrary to linear processes, spatial averaging of nonlinear processes involving local potentials and concentrations is not the same as nonlinear processes under averaged potentials and concentrations. As an example for the latter, one can think of any interfacial reaction that binds lithium ions and leads to battery degradation through SEI growth. If the local environment varies between different locations on an active material particle the amount of consumed lithium can vary as well leading to inhomogeneous SEI. Other examples are localized electrochemical reactions which are initiated only below or above specific values of the electrochemical potential which are not reached homogeneously across the interface. A straightforward attempt to represent these processes in the porous electrode theory by looking at the reaction condition on the surface of the effective spherical particle may lead to biased predictions. Any macroscopic expression theoretically derived based on the microscopic theory has to take into account the distribution of the local fluctuations in the microstructure of the electrodes. The objective of this subsection is to provide a theoretical framework for such description.

The reason why the local spatial distribution of the system variables, such

as overpotential, differs from the smooth prediction of the porous electrode theory lies in the complexity of the microstructure. Figure 1 schematically contrasts the situation in a real microstructure with the representation of this microstructure in the porous electrode theory. We can run a thought experiment in which we transform the latter into the former in a few steps, introducing more realistic structural details to the idealized DFN representation step by step, looking into the changes of the cell dynamics solution that come with it. This transformation is represented in figure 1 when one moves from subfigure C to subfigure A. We have to pay special attention to the quantities that clearly distinguish the porous electrode theory (DFN) solution from the one in the microscopic model. Variation of the variables on the particle-electrolyte interface is one such class of quantities.

In the porous electrode theory (represented by subfigure C of figure 1), the effective particle is put into homogeneous electrolyte media and electric field (in respective phases), disconnected from the other particles. In the first step of the thought experiment (moving to subfigure B), we introduce one change into this idealized system by transforming its shape from spherical to an arbitrary one. The dynamics of the electrolyte and the electric field is kept the same and holds them homogeneous. The ion density in the particle c_s is not constrained and allowed to change in accordance with the diffusion equation. After some time, a region in figure 1, subfigure B with higher interface curvature will typically have higher ion concentration on average than a more flat region. It can be understood if one starts to charge the particle from a state with homogeneous ion density. In such a state the reaction current is the same over the whole electrolyte-particle interface. The average Li ion

density growth rate is then proportional to the surface-to-volume ratio which is locally higher in regions with higher curvature, and this difference will produce a concentration differential. After a period of time, this concentration differential will stop to grow and stabilize due to the diffusion exchange between regions with different concentrations and the self-consistent adaption of the reaction current, thus reaching a steady state. The emergence of stable differences in interface concentrations on the scale of one particle is a clear step away from the assumptions of the porous electrode theory and DFN model where the active material interface is always strictly homogeneous. Inhomogeneous concentration distributions across the interface of the particle will lead to inhomogeneous overpotential distributions via the change in local OCV (see equation (5)) as well.

If one neglects any further differences between the real microstructure environment and the homogenized porous electrode picture as e.g. ion concentration gradients in the electrolyte across the particle size, one obtains basically a modification of the original porous electrode theory, but with the effective particle having an arbitrary shape. In case the control volume contains particles of different shapes, one has to solve the problem for all the particle types or to choose a representative sample of the particle sizes, similar to the way DFN model is generalized by using particle size distributions [23]. The individual diffusion equations for the particles may be solved using, for example, Butler-Volmer expression (4) as boundary conditions with c_e, ϕ_e and Φ_s obtained from the homogenized transport equations of the type of (7). The total current through the interface of all the particles will, in turn, enter these transport equations as a term $\sum n_i I_i$, with n_i being the density of

the i's particle class and I_i - the total current through the particle's interface. To emphasise the close analogy of this model to the DFN model by Newman and the colleagues, we call this ansatz eDFN (extended DFN).

eDFN simplifies the theoretical analysis considerably. In this framework, the difference between the microstructure-resolving model and DFN model is reduced to the difference between transport in a spherical effective particle and in a particles of another geometrical shape. The problem's geometrical domain represents only one particle in the microstructure.

To close the gap between the real microstructure and the porous electrode theory, we return to the thought experiment. We have to add real spatial distribution of the fields $c_e(\vec{r})$, $\phi_e(\vec{r})$ and $\Phi_s(\vec{r})$ and possible ion exchange between different particles. These features are shown in figure 1, subsection A. From the perspective of the c_s dynamics, all these changes can be mathematically understood as modifications in the boundary conditions of equation (8). For example, if one assumes that i_0 behaves according to formulas (4) and (5) then variations in $c_e(\vec{r})$, $\phi_e(\vec{r})$ and $\Phi_s(\vec{r})$ induce variations in i_0. Similarly, one can think about introducing an interparticle contact as going from $i_0 = 0$ in the contact's location there to a finite i_0. Naturally, any variation of i_0 will produce a variation of c_s. When this variation is added to the eDFN solution we come to the exact solution of the microscopic model. To estimate the scale of the difference that comes from it and to support the intuitive cell dynamic picture developed here with mathematics, one needs results of a more rigorous analysis supported with numerical experiments that will be given in the following sections.

2.3. Local fluctuations in the electrode: mathematical theory overview

So far we have outlined how the transition from the homogenized DFN model to the microstructure resolved model can be captured as a change of the shape of the simulation domain and of the boundary conditions for a diffusion equation, and we have seen how it can lead to localized fluctuations of system variables that are not observed in the porous electrode theory. To obtain a more quantitative description, we will now outline a systematic mathematical approach to derive the laws governing the local fluctuations in the electrodes, using homogenization theory, perturbation ansatz and asymptotic analysis of partial differential equations (PDE). The details of the derivation will be published separately since we concentrate here on the general structure of the theory and the most important new results. We also will not cover the topic of how exactly and under which conditions the microscopic model fully converges to DFN model, because this question, however important on its own right, is not directly relevant to our goal of understanding the local fluctuations in porous electrodes on a particle scale.

To this end, we will proceed as follows. First, we will identify the small dimensionless parameters that characterize an electrode, then we will demonstrate how it will lead to a simplified equation that correspond to the zeroth-order approximation relative to these parameters. These equations correspond to eDFN model. Then we will introduce further simplifications through making eDFN linearized. For this latter model, we will show which parameters influence the scale of local fluctuations and how, and why the assumptions that we make while deriving the model are justifiable. This is a move in the direction opposite to the one in section 2.2, where we turned

DFN model into the microscopic model by adding features incrementally. In figure 1, it means moving in the direction from subfigure A to subfigure C.

We begin with the small parameter identification. We propose that the ratio of typical microstructure length scale to typical macroscopic length scale is one such parameter. The typical microstructure length is of the order of active material particles size L. The macroscopic length scale L_0 is the one on which variation of either one of quantities ϕ_e, Φ_s or c_e is of the order of their average values. This length depends inversely on their gradients and does not necessary correspond to the electrode thickness, the later rather serves as a physics-motivated lower bound of the former, because otherwise regions of lithium depletion in the electrolyte occur. We assume that no realistic cell works under such conditions. As a result, we can assume that the parameter

$$\delta_1 = \frac{L}{L_0} \tag{10}$$

is indeed small when the electrode's thickness contains multiple active material particles.

Another small parameter is the ratio of the interparticle interface surface area to the total surface area of the particles in the microstructure:

$$\delta_2 = \frac{S_{interparticle}}{S}. \tag{11}$$

The assumption that the parameter is small means that the microstructure domain corresponding to the active material can be reasonably split into weakly connected subdomains-particles.

To proceed with the argument, we propose that a perturbation ansatz is applicable and that a solution of the microscopic model (1-3) can be resolved

into power series of δ_1 and δ_2:

$$\begin{aligned}
\phi_e &= \phi_e^{(0)} + \phi_e^{(1)} + ..., \\
c_e &= c_e^{(0)} + c_e^{(1)} + ..., \\
\Phi_s &= \Phi_s^{(0)} + \Phi_s^{(1)} + ..., \\
c_s &= c_s^{(0)} + c_s^{(1)} + ...,
\end{aligned} \tag{12}$$

where the quantities with index 0 correspond to the zeroth-order terms and the quantities with index 1 are linear with respect to δ_1 and δ_2.

The expansion of ϕ_e, Φ_s and c_e into power series of δ_1 is covered in the homogenization theory, the field of mathematics that describes how one can scale up differential equations in the systems with scale separation either in space or time or both. The spatial scale separation holds when δ_1 is small and the problem time scale is sufficiently large. The details of this framework's application to Li-Ion cells are described in [18, 19, 20]. Here, the authors mathematically demonstrated that the equations of the DFN model can be rigorously derived in the limit $\delta_1 \to 0$. If one does not consider the δ_2 part of the expansion for a while, it means that $\phi_e^{(0)}$, $\Phi_s^{(0)}$ and $c_e^{(0)}$ from the series (12) are the solutions of the corresponding homogenized DFN equations.

Li concentration in active material c_s is a special case. For homogenization to be applicable, the time scales of the processes in the microstructure should be smaller than the characteristic problem time. Their ratio should, strictly speaking, be used as an additional small parameter in the expansion (12), we will not do it to spare additional notations. The time scale separation typically does not hold for the lithium transport in the active material phase. As a consequence, the homogenized mass transport equation for c_s

will actually not be accurate when $\delta_1 \to 0$. This fact was demonstrated using numerical simulation in [20]. As a result, the accurate PDE problem for $c_s^{(0)}$ is still (8). As we saw in sections 2.1 and 2.2, DFN bypass this caveat of not-homogenized Li transport by substituting the microstructure complexity with that of the effective spherical particle problem (9), making the model more intuitive and computationally robust, yet less accurate, and eliminating any surface fluctuations on the way.

From this point we will outline our novel results that go beyond the standard homogenization procedure. We have developed a proper perturbation ansatz with both parameters δ_1 and δ_2 kept small but finite.

The functional form of the equations for $\phi_e^{(0)}$, $\Phi_s^{(0)}$ and $c_e^{(0)}$ is still kept to be the homogenized transport equations from DFN model. $c_s^{(0)}$ remains a solution of (8) as well, with minor change in the boundary conditions that do not affect the further results. The PDE problems for $\phi_e^{(1)}$, $\Phi_s^{(1)}$ and $c_e^{(1)}$ in our theory are identical to the auxiliary cell problems used in the homogenization theory (see [19, 18, 20] for the details). In the case of $c_s^{(1)}$, an important observation simplifies the problem. Normally, in the schemes using perturbation technique, zeroth-order problems are solved separately and then their solutions are used as parameters for first-order perturbation problems and so on. The later can not be generally split further into sub-problems.It would mean that the PDEs for $\phi_e^{(1)}$, $\Phi_s^{(1)}$, $c_e^{(1)}$ and $c_s^{(1)}$ are coupled with each other. In our case, homogenization theory shows that the equations for $\phi_e^{(1)}$, $\Phi_s^{(1)}$ and $c_e^{(1)}$ are decoupled and do not include $c_s^{(1)}$. Hence, the problem for $c_s^{(1)}$ can be consistently solved with $\phi_e^{(1)}$, $\Phi_s^{(1)}$ and $c_e^{(1)}$ just as parameters, not

variables. The resulting PDE for $c_s^{(1)}$ is

$$\begin{aligned}
\frac{\partial c_s^{(1)}}{\partial t} &= \vec{\nabla}(D_s \vec{\nabla} c_s^{(1)}), \\
D_s \frac{\partial c_s^{(1)}}{\partial n} &= \frac{1}{F} \Bigg(- \frac{\partial i_0 \left(\phi_e^{(0)}, \Phi_s^{(0)}, c_e^{(0)}, c_s^{(0)} \right)}{\partial c_s} c_s^{(1)} \\
&\quad - \frac{\partial i_0 \left(\phi_e^{(0)}, \Phi_s^{(0)}, c_e^{(0)}, c_s^{(0)} \right)}{\partial \phi_e} \phi_e^{(1)} - \\
&\quad - \frac{\partial i_0 \left(\phi_e^{(0)}, \Phi_s^{(0)}, c_e^{(0)}, c_s^{(0)} \right)}{\partial \Phi_s} \Phi_s^{(1)} - \\
&\quad - \frac{\partial i_0 \left(\phi_e^{(0)}, \Phi_s^{(0)}, c_e^{(0)}, c_s^{(0)} \right)}{\partial c_e} c_e^{(1)} - \\
&\quad - i_{ip}) \text{ on the interface.}
\end{aligned} \tag{13}$$

The term i_{ip} represents the possible inter-particle current, it does not depend on $c_s^{(1)}$. The decoupling of $\phi_e^{(1)}$, $\Phi_s^{(1)}$, $c_e^{(1)}$ from $c_s^{(1)}$ also implies that the terms $\frac{\partial i_0 \left(\phi_e^{(0)}, \Phi_s^{(0)}, c_e^{(0)}, c_s^{(0)} \right)}{\partial \phi_e} \phi_e^{(1)}$, $\frac{\partial i_0 \left(\phi_e^{(0)}, \Phi_s^{(0)}, c_e^{(0)}, c_s^{(0)} \right)}{\partial \Phi_s} \Phi_s^{(1)}$, $\frac{\partial i_0 \left(\phi_e^{(0)}, \Phi_s^{(0)}, c_e^{(0)}, c_s^{(0)} \right)}{\partial c_e} c_e^{(1)}$ do not depend on $c_s^{(1)}$, neither explicitly nor implicitly. The problem (13) is defined on the domains corresponding to all the particles in the system individually.

In the rest of the paper, we will mostly investigate the properties of $c_s^{(0)}$. Both $c_s^{(0)}$ and $c_s^{(1)}$ can contribute to the surface fluctuations, which is the main topic of this paper, and the respective contributions will be compered at the section's end.

Setting δ_1 and δ_2 to zero, the problem (8) for every active material particle combined with the homogenized equations for potential and electrolyte concentration constitute eDFN model as defined in the previous section. The condition $\delta_1 = 0$ is the limit of absolute length scale separation and is equi-

valent to the fields Φ_s, c_e and c_s being homogeneous on the particle scale. $\delta_2 = 0$ is equivalent to preventing any exchange of lithium between particles.

To extract further useful information from eDFN model, we will linearize the concentration dependence of the exchange reaction current: $i_0 = \alpha + \beta c_s^{(0)}$. The accuracy of such an approximation will be briefly discussed at the end of the section. The solution of the resulting linear non-homogeneous PDE problem in an active material particle

$$\begin{aligned} \frac{\partial c_s^{(0)}}{\partial t} &= \vec{\nabla}(D_s \vec{\nabla} c_s^{(0)}), \\ D_s \frac{\partial c_s^{(0)}}{\partial n} &= -\frac{1}{F}\left(\alpha + \beta c_s^{(0)}\right) \text{ on the interface,} \end{aligned} \tag{14}$$

can then be used to solve for the fluctuations $c_s^{(1)}$ (equation (13)).

Equation (14) has a number of useful mathematical properties. If one assumes that β is independent of time and non-negative, and α depends on time such that constant total current is ensured (i.e. galavanostatic charge/discharge for every individual particle), one can show that the problem has an asymptotic solution of the following form for $t \to +\infty$:

$$c_s^{(0)} \simeq C_0 - \frac{\overline{i_0} t S}{FV} + \Delta c_s \tag{15}$$

where $\overline{i_0}$ is the average current, which is constant, and S and V denote surface area and volume of the particle respectively. The terms $C_0 - \overline{i_0} t S/FV$ represent the overall charge level of the particle changing linearly with time (in this paper, we define the ion current directed from the particle to be positive, consistent with our definition of Butler-Volmer expression and the overpotential). They do not depend on coordinates. The term Δc_s, to the contrary, depends on coordinates, but is independent of time. The possibility

of such split is the defining property of the asymptotic solution. One may notice that the separation of the solution into the coordinate-dependent and time-dependent parts is not unique: a constant can be added to one part and be subtracted from the other. We remove this degree of freedom by setting the volume average of Δc_s to be zero:

$$\int \Delta c_s dV = 0. \tag{16}$$

In plain English, the asymptotic solution is a sum of the overall level of particle lithiation plus a stationary geometric profile of the concentration gradients.

The results that we present further are derived as the properties of Δc_s. By definition, this coordinate-dependent paprt contains all the information about the local spatial fluctuations, which are the main object of interest in this paper. First, some notes should be made regarding its relation to the general solution of (14). When a cell undergoes charge-discharge under various protocols, the total current running through every particle is not constant in general even when the current through the whole cell is constant. There is also no reason to expect β to be constant. However, the general solution gravitates toward the stationary solution, and we make a conjecture that, for our purposes, the former can be approximated by the latter with $\beta = \beta(t)$ and $I = I(t)$. When β and $\overline{i_0}$ change slow enough, the exact solution changes adiabatically with the stationary solution. The asymptotic approach toward the stationary solution has the time scale equal to the diffusion time of the problem, the analysis of the numerical simulations whose results will be presented in below in the text suggest that quite often for the distribution of c_s along the surface the equilibration happens even faster. A reliable rule of

thumb is that the higher current/C-rate is, the further away are the profiles of $c_s^{(0)}$ and of Δc_s.

Having said this, we narrow down our analysis to the properties of the stationary solution. The dimension analysis allow to write the dependence of Δc_s on coordinates as follows:

$$\Delta c_s(\vec{x}) = \frac{\overline{i_0}L}{FD_s} f\left(\vec{x}/L, \frac{\beta L}{FD_s}\right). \tag{17}$$

Here, L is a typical linear size of the particle. If β and D_s are not constant one has to use the corresponding averages. Properly defined, function $f(...)$ is dimensionless and depends only on the shape of the particle. Based on (17), it can be observed that any homogeneous functional of degree 1 over $\Delta c_s(\vec{x})$ can also be written in specific form. One such functional is a standard deviation of $\Delta c_s(\vec{x})$ on the particle surface:

$$\begin{aligned} \delta c_s^{(0)}|_S &\equiv \left(\int \frac{dS}{S}\left(\Delta c_s - \overline{\Delta c_s}|_S\right)^2\right)^{1/2} = \frac{|\overline{i_0}|L}{FD_s} f_1\left(\frac{\beta L}{FD_s}\right), \\ \overline{\Delta c_s}|_S &\equiv \int \frac{dS}{S}\Delta c_s, \end{aligned} \tag{18}$$

where $f_1(...)$ is another dimensionless shape-dependent function. The expression for $\delta c_s^{(0)}|_S$ is extremely relevant for understanding how the surface fluctuations of c_s behave. In a spherical fully isotropic particle $\delta c_s^{(0)}|_S \equiv 0$ hence $f_1(...) \equiv 0$.

The form (17) of the solution's presentation naturally leads to a conclusion that the expressions $|\overline{i_0}|L/FD_s$ and $\beta L/FD_s$ are two main parameters that characterize the dynamics of the particle's lithium concentration gradients and contrast them with those of the other particles. Let us have a closer look at these parameters. $|\overline{i_0}|L/FD_s$ has the dimension of concentration and

can be equivalently rewritten as $c_m|\overline{i_0}|/i_{cr}$, where c_m is the maximal possible concentration of lithium in the active material under consideration and $i_{cr} = FD_s c_m/L$ is an estimate of the critical current density above which the transport limitation blocks charge or discharge. So, under save cell operation regime, maximum $|\overline{i_0}|L/FD_s \sim c_m$.

For the second parameter, which is dimensionless, we introduce a notation

$$\rho = \beta L/FD_s. \tag{19}$$

Its meaning will become clear when we first look at the asymptotic cases of (17) and (18) at $\rho \to 0$ and $\rho \to +\infty$. We have shown that when $\rho \to 0$

$$\delta c_s^{(0)}|_S \simeq \gamma_1 \frac{|\overline{i_0}|L}{FD_s}, \tag{20}$$

and when $\rho \to +\infty$

$$\delta c_s^{(0)}|_S \simeq \gamma_2 \frac{|\overline{i_0}|L}{FD_s\rho} = \gamma_2 \frac{|\overline{i_0}|}{\beta}, \tag{21}$$

where γ_1 and γ_2 are the dimensionless numbers characteristic of the particle's shape. The comparison of the formulas (20) and (21) demonstrates that variation of concentration on the surface tends to decrease at least when ρ becomes sufficiently big. Numerical tests (see the next section) demonstrate that for spheroids this trend actually holds for almost all the values of ρ. Notoriously, both asymptotic limits depend either on β or on D_s but not on their combination.

Is it simply a coincidence? Let us return to the thought experiment from the previous section, when we considered charging an active material particle of a non-spherical shape starting from a homogeneous lithium distribution, in homogeneous electrolyte and without gradients in electric potentials in the

vicinity. Two forces were mentioned that smooth the buildup of the gradients between the different regions of the particle: dependence of the intercalation current on lithium concentration and diffusion between regions with different concentration. In the context of PDE problem (14) these two factors are represented exactly by the respective parameters β and D_s. We hypothesised that a stationary gradient profile would appear in which these two factors are in a dynamic equilibrium with the factor of local surface curvature difference that makes the local concentration values move away from one another. Closer look at the formulas (20) and (21) reveals exactly such phenomena: in both the concentration variation inversely depends on β or D_s, thus justifying the observation that those factors indeed suppress the variation of c_s on the surface. At this point, the two presented pictures i.e. the mathematical route from the microscopic model up to DFN model and the qualitative description of generalizing DFN to the exact microstructure and electrolyte description meet each other.

In this context, parameter $\rho = \beta L/FD_s$ can be understood as a ratio of the relative contributions of the factors β or D_s to the local fluctuations. Small ρ can be thought as corresponding to a fast diffusion regime: the local inhomogeneities are smoothed out by intensive diffusion before any dependence of the intercalation current on lithium concentration becomes important. Mathematically, β disappears from (20). Inversely, big ρ is a slow diffusion case: the local feedback of the growing c_s on the reaction current i_0 suppresses the concentration gradient buildup before the diffusion flux starts to play any role. To reflect it, no dependence on D_s in (21) appears.

Those are the main mathematical features of the theory that one needs

to understand the numerical results of the following section. Here, we still have to add a few useful comments. First, the question of accuracy when one substitutes the problem (8) with its linear counterpart (14): it can be demonstrated that the implicit perturbation series, that we get by dropping the nonlinear part of $i_0(c_s)$, do not generally lead to secular perturbation terms, i.e. the terms that, being small at one moment, may grow unrestrained later.

Second, we return again to the first-order perturbation solution $c_s^{(1)}$. The mathematical forms of the equations (13) and (14) are identical (which follows from the fact that, as it was emphasized, in the complete close model, $c_s^{(1)}$ influences only the terms in which it is explicitly included). Using the same theory, we come to similar laws governing the influence of, for example, homogenized gradient of electrocheimical potential on the local fluctuations of c_s on the particle interface:

$$\delta c_s^{(1)}|_S \simeq \frac{L\frac{\partial i_0}{\partial \phi_e}\delta\phi_e|_S}{FD_s} f_2(\rho) \sim \frac{L|\overline{i_0}|\delta_1}{FD_s} f_2(\rho). \tag{22}$$

or of the interparticle Li exchange current i_p:

$$\delta c_s^{(1)}|_S \simeq \frac{L\delta_2|i_p|}{FD_s} f_3(\rho). \tag{23}$$

$\delta\phi_e|_S$ is a standard deviation of ϕ_e on the particle's surface, defined in the same manner as $\delta c_s^{(0)}|_S$ in formula (18). Similarity to (18) is easy to observe. We introduced new dimensionless functions $f_i(...)$ that are not identical to $f_1(...)$ from (18). They do not generally become zero for spherical isotropic particles, for example. Yet, the asymptotic behaviour with respect to ρ follows the same trends like (20) and (21).

We explicitly included the parameters δ_1 and δ_2 into (22) and (23), to compare these formulas with (18). All the fluctuations of c_s due to the first-order perturbation terms become zero in the limit $\delta_1, \delta_2 \to 0$, contrary to equation (18), where the formula do not contain δ_1 or δ_2. In plain English, this important observation states that, even in the case of an electrolyte with an extremely fast electric and mass transport, local fluctuations of c_s on active material-electrolyte interface do not generally become zero. Surface fluctuations of ϕ_e, Φ_s and c_e appear only in the first-order perturbation terms and become zero when $\delta_1 \to 0$. Despite the contributions to c_s from the first-order perturbation terms being generally small at small but finite δ_1 and δ_2, they can still be comparable to $\delta c_s^{(0)}|_S$ when the microstructure is built of spherical or almost spherical particles, for which function $f_1(...)$ in the expression (18) is zero or very small. As we will see in the next section, in a more general case and for the parameters typical for lithium-ion electrodes, the contribution from $c_s^{(0)}$ is significantly more pronounced. One can not also exclude the possibility that $c_s^{(1)}$ can play a more visible role in complex electrodes containing regions with very high tortuosity.

Finally, an additional connection can be established between the formulas above and the physical characteristics of electrodes. For this, we adopt the specific form of the $i_0(c_s)$ law - Butler-Volmer formula (4). It can be shown then, that when a particle undergoes galvanostatic charge/discharge β is roughly proportional to the slope of OCV curve, with the exceptions of the regions near the edges of the SOC range where the pre-exponential terms in (4) have singularity. When it holds, the asymptotic formulas (20) and (21)

can be rewritten in terms of the OCV slope $\delta U_0/\delta c_s$:

$$\delta c_s^{(0)}|_S \sim const \tag{24}$$

when $|\delta U_0/\delta c_s| \to 0$ and

$$\delta c_s^{(0)}|_S \sim \frac{1}{\frac{F}{RT}|\delta U_0/\delta c_s|} \tag{25}$$

when $|\delta U_0/\delta c_s| \to +\infty$. The next section will demonstrate numerically that the inverse dependence between $\delta c_s^{(0)}|_S$ and $\delta U_0/\delta c_s$ holds not only asymptotically but with finite values of the OCV slope. The zeroth-order contribution to overpotential under the same assumptions has exactly the opposite dependence on $\delta U_0/\delta c_s$: when $|\delta U_0/\delta c_s| \to 0$

$$\delta \eta^{(0)}|_S \sim |\delta U_0/\delta c_s|, \tag{26}$$

and when $|\delta U_0/\delta c_s| \to +\infty$

$$\delta \eta^{(0)}|_S \sim const. \tag{27}$$

In case of the first-order perturbation with finite but small δ_1 and δ_2, no similar clear monotonous dependence of $\delta \eta^{(1)}|_S$ on $|\delta U_0/\delta c_s|$ or β can be theoretically justified on the same level of generality.

3. Numerical simulation results and discussion

3.1. Numerical simulation methods

We use the finite volume implementation of the microscopic model in the software package BEST (Battery and Electrochemistry Simulation Tool [24]. Besides this, we will use isolated one-particle finite volume simulations. They are implemented using Scipy Python packages.

3.2. Simulation results and discussion

From the analysis in the previous sections we saw that out of the four variables that describe the state of the cell in the microscopic model, the surface fluctuations of c_s are the ones that may not become negligibly small even when particle and scale separation conditions hold ($\delta_1, \delta_2 \ll 1$). More specifically, we draw the following conclusions: (a) the scale of these fluctuations is mainly defined by the shape of the particle, total current through the surface and slope of the reaction current dependence on c_s, (b) the fluctuations' dependence on these quantities follows some specific laws (formulas (20) and (21)), (c) there is no significant influence from nonhomogeneous distribution of electrolyte lithium concentration and of electric potential. Having to introduce a number of assumptions in the derivation, one has to utilize numerical simulation tests to find out, to which extent these theoretical findings apply to real cells and within the corresponding parameter range. This is the objective of this section.,

We begin with the numerical simulations of the PDE problem (14). Our goal is to obtain the dependence of the surface c_s fluctuation scale on the particle's shape and on parameter ρ. We solve the problem (14) on different spheroid particles, each characterized by its aspect ratio ε. The main axis length L is always kept equal to 10 µm, lithium diffusion coefficient D_s is $10^{-10}\ cm^2\ s^{-1}$, and these two quantities are used in the definition of ρ according to (19). For the boundary condition, we keep the current density fixed and equal $\widetilde{i}_0 = -2 \cdot 10^{-4} A/cm^2$ ("$-$" sign in our convention means that lithium goes into the particle) at a certain point on the surface $\vec{x}_0$. Then,

everywhere else the current i_0 should be calculated as

$$i_0 = \widetilde{i}_0 + \beta(c_s - c_s(\vec{x}_0)) \tag{28}$$

to fit into the class of linear boundary conditions of (14). We use a heuristic rule to choose mesh resolution for every specific simulation run. The rule will be explained later, because for this an additional analysis of the solution is needed, which will be given below, after the results are presented.

The parameters have been chosen to closely represent graphite being charged with the current close to the critical one. Following the methods we used in the theoretical analysis, we look to compare the concentration profiles of the stationary solutions that emerge after a period of time. With graphite-like OCV curve and Butler-Volmer formula, direct tracking of the relation between c_s variation and parameter ρ (or β) is hard, which motivates to choose the artificial kinetic law (28). To ensure that the transient processes have ended, we let the simulation run for roughly two diffusion times L^2/D, after which the stationarity of the profiles was checked. Figure 2 demonstrates the examples of the concentration profiles. Figures 3 and 4 display the dependence of the total variation (maximum minus minimum) of the lithium ion concentration on the surface of the particles against ε and ρ.

Figure 4 demonstrates the behaviour of concentration variation that agrees with the trend predicted by formulas (20) and (21): it monotonously decreases when ρ becomes big. As one can see, for spheroids this dependence holds not only when $\rho \to \infty$ but effectively for all values of ρ, as it was indicated in section 2.3. In figure 3, the variation decreases with $\varepsilon \to 1$ that corresponds to spherical particle shape. The behaviour near $\varepsilon = 0$ demonstrates a peculiarity. Below $\varepsilon = 0.2$ the trend depends on ρ: for $\rho > 5$ the variation increases

with ε, for $\rho < 1$ it decreases. We argue that it can be explained through the properties of the base PDE problem (14) in the following way. Spheroids with small ε are close to one-dimensional systems (like the particle at the bottom of figure 2), and the corresponding solution can be approximated by the solution of a one-dimensional equation obtained by averaging of the problem (14) with the boundary condition current (28) over the cross sections perpendicular to the main axis. The resulting one-dimension equation is

$$\frac{\partial c_s}{\partial t} = \frac{\partial}{\partial x}\left(D_s \frac{\partial c_s}{\partial x}\right) - \frac{l(x)}{FS(x)}\left(\widetilde{i}_0 + \beta(c_s - c_s(x_0))\right). \tag{29}$$

$S(x)$ is the surface area of the cross section, $l(x)$ is the length of its contour. Both of the parameters are assumed to depend on x based on the exact shape they are calculated from. For a specific case of ratio $l(x)/S(x)$ and D_s being independent of x an analytical solution can be written down, including the stationary solution. Parameter $\widetilde{\varepsilon} = SL/l$ is close to the aspect ratio ε of our simulation problem, and a more detailed analysis can be carried out for the cases $\widetilde{\varepsilon} \gg \rho$ and $\widetilde{\varepsilon} \ll \rho$ even when $l(x)/S(x)$ and D_s depend on x. In particular, when $\widetilde{\epsilon} \ll \rho$, the variation of the stationary solution is mainly present near the edges of quasi-one dimensional particle, penetrating on the length scale $\Delta l \sim \sqrt{DS/l\beta} = L\sqrt{\widetilde{\varepsilon}/\rho}$. The c_s variation itself scales with $\widetilde{\varepsilon}$ as $(\widetilde{\varepsilon}/\rho)^{0.5}$. This trend corresponds qualitatively to the points on the graph of figure 3 with $\varepsilon < 0.2$ and $\rho > 5$. The exact quantitative agreement with the law $(\widetilde{\varepsilon}/\rho)^{0.5}$ may not hold, at least because the approximation or quasi-one dimensional body may not be valid at edges or due to some numerical artifacts. We find, however, the combination of the simulation data with such heuristic mathematical analysis lead to a solid conclusion that squeezing particles do not lead to bigger overall surface fluctuations of c_s, and the

general rule, that the further particle shape is away from isotropic spherical, the more pronounced the fluctuations are, does not hold for $\rho \gg \varepsilon$.

The concentration distribution snapshot on the right side of figure 2 corresponds exactly to the case $\rho \gg \varepsilon$. One can notice that, indeed, most of the variation is localized near the edges of the particle, producing a type of skin effect. The emergence of an additional length scale Δl may affect the quality of the solution in the finite volume method. This observation returns us to the rules for choosing mesh resolution for the problem (14) whose description was postponed. They should incorporate the knowledge about the new length scale. For this research, we choose the mesh resolution in such way that the particle length has at least 40 control volumes (CVs) and Δl for the maximal possible ρ has at least 3 CVs.

Now, we have demonstrated that the numerical simulation results agree with the part of the theory reflected in conjecture (b) from the beginning of the section, for cell models in which parameter ρ can be set and controlled manually. In cells with real parameters, such explicit test is harder due to the information about the parameters being hidden in the dynamics and them being entangled with each other. Nevertheless, a qualitative analysis is still possible. For this, we will analyse a full microstructure-resolving simulation. Then, to test the prediction that influence of non-homogeneous electrolyte on the c_s fluctuations scale is negligible (conjecture (b) and formula (22)), we will compare the microstructure-resolving simulation with a number of reference simulations.

In this simulation, a numerical model of the electrode is build from spheroid particles with aspect ratio 0.5 that are connected by small conductive

non-intercalating material beams along the major axes. These complexes are bound to a current collector with another conductive material beam. The electrode is built out of $3 \times 3 = 9$ such complexes, each having 3 particles, and is a periodic system of 27 individual particles (see figure 5, the conductive material is not shown). We ran galvanostatic charge simulation within a half-cell setup using the the microscopic model (equations 1-3). The dimensions of the cell are 34.5 μm×17.25 μm×17.25 μm, the spheroid's main axis size is 10 μm and the diameter of the conductive material bridges connecting the spheroids is 0.5 μm. The physical parameters of the cell's components are listed in Table 1. The chemical potential of the electrolyte lithium is calculated according to the ideal solution theory. The OCV vs. SOC function is

$$\begin{aligned} U_0(SOC) =& 0.6379 + 0.5416 \cdot \exp(-305.5309 \cdot \mathrm{SOC}) + \\ &+ 0.044 \cdot \tanh(-(\mathrm{SOC} - 0.1958)/0.1088) - \\ &- 0.1978 \cdot \tanh((\mathrm{SOC} - 1.0571)/0.0854) - \\ &- 0.6875 \cdot \tanh((\mathrm{SOC} + 0.0117)/0.0529) - \\ &- 0.0175 \cdot \tanh((\mathrm{SOC} - 0.5692)/0.0875) \end{aligned} \tag{30}$$

The separator consists of pure electrolyte. The parameters for the active material particles are chosen to be close to the ones of graphite, the conductivity of the bridges $\sigma^{(additive)}$ is set to be high enough, so they don't play any dynamical role other then to provide electric contact. The side walls of the simulation box have periodic boundary conditions.

As a first reference system, we did a charge simulation of one particle with the same geometrical, physical parameters and mesh discretization in eDFN

framework, i.e. with homogeneous ϕ_e, Φ_s and c_e. To imitate the galvanostatic constraint on the original cell, we set the current through our particle to be the total current through the original cell divided by the number of particles, i.e. 27.

One can visually examine in a concentration snapshot in figure 5 that the lithium profile in different particles evoleves almost in unison, indirectly justifying the use of one-particle eDFN model. Figure 6 shows the evolution of the total variation of the surface lithium concentration and overpotential. It demonstrates a good quantitative agreement with the results of the eDFN simulation. We plotted the OCV slope evolution in the same figure below. The comparison of the curves confirms the conjecture from the end of the previous section about the inverse dependence between the amplitude of concentration variation and the slope of OCV (equations (24) and (25)). Similarly, the overpotential variation evolution follows the trend based on equations (26) and (27): the overpotential spread is higher when the OCV slope is steeper. In both figures a slight deviation between the eDFN's and the microstructure theory curves can be seen closer to the end of the charge. It may be due to the fact that the behavior of the current function i_0 from the boundary conditions between the phases becomes strongly nonlinear near the SOC points 0% and 100%, due to singularities in either OCV or in the preexponential term of Butler-Volmer formula: it may lead to the situation when many of the assumptions, that we made in the previous section to justify the use of eDFN model and of the homogenization theory, break, and the conclusions we derived from them may stop being valid too.

According to the definitions of the section 2.3, the first one-particle refe-

rence system represents the zeroth-order solution $c_s^{(0)}$. It means a comparison with the exact microstructure solution will allow us to estimate the scale of $c_s^{(1)}$ and its contribution to the surface fluctuations. One of the ways to demonstrate the difference is to look at the surface c_s variation on different particles from the electrode in figure 5. In the electrode, we separately analyzed 3 layers of particles lying on top of each other. We tracked the total surface variations of c_s in each of those layers. There are two factors that make the layers not equivalent to each other: the slight variation of c_e, ϕ_e and Φ_s from layer to layer and the different way in which the conductive material is connected to the particles. The first layer is connected only from one side while the remaining two from both, at the same time the variations of the ion concentration in the electrolyte and the potentials in principle can be different for all the layers. In figure 6, the evolution of total surface variation of c_s and of overpotential η respectively are presented, for the exact microstructure simulation, integral and for each of 3 layers, and for the reference system. All the curves agree with each other qualitatively. Especially noticeable is the fact that the total variations for the two closest to the current collector layers are very close, almost indistinguishable. These two layers geometrically are the exact copies of each other, each bound to two conductive bridges above and below. The only thing that differentiates these two layers during the charge is the local variation of the fields c_e, ϕ_e and Φ_s. In our theoretical framework, the contribution of such variation is represented by the formulas like (22). Our basic theoretical analysis left the question open how small the first-order perturbation contribution to the surface fluctuations within the parameter range of real cells is, and the data in

figure 6 provides a numerics-backed answer. The clear monotonous behavior of $\Delta\eta$ with OCV slope mentioned above can be understood as a necessary condition and thus hint for the small role of the first-order perturbation, as follows from the theoretical results (comments about $\delta\eta^{(1)}|_S$ after formulas (26) and (27)).

To further investigate the correctness of the negligible nonhomogeneous electrolyte role assumption, a second reference system's charge was simulated. This cell has all the geometry and the parameters of the original, except for D_s and κ_e, which are multiplied by 100. If one neglects the nonlinearities of flux and current laws 2, it effectively makes all the gradients in electrolyte roughly 100 times smaller, or, following the way we defined small parameter δ_1, makes the latter 100 smaller too. According to the formula (22), the contribution of the gradients to the surface fluctuations should decrease by factor 100 as well. It is indeed what we observe qualitatively in figure 7 where the total variation evolution again split into layer contributions, but for the second reference system. With the same general scale, the contributions of two lower layers became even more indistinguishable.

Next, we simulated a third reference system, whose difference from the original is that the frontal parts of the spheroid particles of the first layer are covered with plugs made of the same conductive material as the bridges connecting the particles (figure 8). There, the particles of all 3 layers are absolutely geometrically identical. Figure 9 with the evaluations of all the layers' surface variations demonstrates that, as it can be predicted in our theory, all these variations are almost identical.

Finally, we produced a fourth reference system electrode in which, simi-

larly to the one in figure 8, all the particle are equivalent with each other in terms of their shape and their interface with the electrolyte, but the particle orientation relative the cell throughput direction is different (see the charge snapshot in figure 10). Here, it is achieved as well with the symmetrical addition of the conductive additive. Again, visually all the individual particle concentration profiles are very similar, as one would expect. One has to note that the particles are not equivalent in this sense to the ones in figure 8 because the connection of the conductive bridges happens in another location on the surface. We expect the difference between the fluctuations in these two systems to be similar to the difference between the front and the back layers in figure 6, where it is due to similar variation in the conductive material-active material interface. Indeed, this similarity can be observed in figure 11, where we compare the surface concentration variations of the electrodes from figure 8 and 10). We plotted the comparison of two fluctuation measures: standard deviation from equation (18) and total variation. The relative difference between total variations is bigger because this measure is more sensitive to the local differences near extreme concentration values, whereas, in the standard deviation, their scale is compensated by a small share of the surface area on which they occur.

To sum up, the numerical experiments supported the conjecture (c) in which we stated that, for electrolytes, microstructure geometry and active materials typical for real cells, the contribution of nonhomogeneous fields c_e, ϕ_e and Φ_s associated with the first-order perturbation $c_s^{(1)}$ in our theory, is small enough to justify dropping it from the future surface fluctuation model development. The zeroth-order contributions to the fluctuations are coupled

only to the solution of the homogenized DFN equations making the whole model more computationally robust and intuitive. We do not exclude, however, that for more complicated microstructures, possibly with big tortuosity, $c_s^{(1)}$ play a more visible role. Yet, in our opinion, keeping only $c_s^{(0)}$ will still remain a good approximation. We also observed that the geometrical factor next in importance to the particle shape in terms of the influence on the fluctuation scale is the structure of the (conductive) additive material/active material interface.

To deepen the connection between our new analysis and the existing research, we want to discuss how our results are related to the ones in [2], which served as a starting point for the investigation in this paper. The local fluctuations of overpotential observed in the simulation results there may lead a reader to the conclusion that they follow a certain stochastic law. The microstructure in [2] is build of the particles of the same geometry, but connected to each other in a random manner. Our analysis so far, both theoretical and numerical, suggests that, to the contrary, fluctuation profiles of all similar particles should be similar and evolve in a deterministic manner. We think, that the visual randomness of the data in [2] is rather a sort of visual illusion: the noisy image is a result of the superposition of quite deterministic single-particle contributions, with only the particle positions and orientations being random.

To demonstrate this, we ran a simulation of a half-cell with the parameters in Table 1, but with a different geometry (figure 12): the electrode is made of the same spheroid particles as our initial electrode model, but the locations of the particles are defined according to a random rule. Conductive material

bridges connect the particles. Figures 13 and 14 demonstrate the projections of the concentration and the overpotential fields on the particle interfaces in the middle of the charging process for the cells in figure 5 and figure 12 respectively. In the former, the profiles from different particle layers are clearly distinguishable, while in the latter they overlap producing a slightly more chaotic pattern. When one looks at the 3D concentration snapshot in figure 12, one sees, however, the same dynamics as in the simulations above: the particles with the same geometry evolve essentially in unison.

4. Conclusions

The main subject of this paper is the theory of particle scale-localized spatial fluctuations of physical quantities (ion concentrations and potentials) in electrode microstructures. This type of fluctuations was observed in the numerical simulations based on a microstructure-resolving model [2], particularly in the form of overpotential fluctuations. Interestingly, it was also demonstrated in [2] that a running average of the fluctuating results agrees as expected very well with the homogenized DFN model whereas all overpotential fluctuations around the DFN mean vanish upon averaging. It turns out that the decisive difference between DFN and microscopic models is due to the inherent geometric symmetry of the former (effective spherical particle as an active material model). Yet, non-uniform distribution of local physical variables on the electrolyte-active material interface may influence the properties of a battery as a whole, since e.g. the initiation of degradation processes will critically depend explicitly on the local interface environment. This is the very nature of electrochemical reactions, which cannot be ful-

ly captured by a global, homogenized cell description. Our extension of the DFN-type models aims for keeping their computational efficiency but capturing microstructure induced local fluctuations of electrochemically relevant quantities approximately.

In order to identify the origin of the observed fluctuations, we are approaching the problem step by step from a mathematical point of view, rigorously tracing the transition from microstructure based models to DFN through introduction and testing of well defined mathematical approximations. The first approximation is a requirement of spatial scale separation between the particle and the macroscopic electrode scale i.e. parameter δ_1 in our notation should be small. This is the standard starting point of homogenization theories[18, 19, 20], but it turns out that the approach breaks for mass transport in the active materials. To extend the standard approach and in order to test quantitatively the importance of inter-particle contacts, we proceeded further by considering a representation of the electrode as a sum of independent particles in homogenized electrolyte and electric field but allowing contact as perturbations. To quantify the accuracy of this model, we introduced a new parameter δ_2 as a ratio of inter-particle interface surface area with ion transport to the total surface area of the particles. The requirement that δ_2 is small is the second approximation that we impose on the initial microscopic cell model. The resulting mathematical framework for cases when $\delta_1, \delta_2 \to 0$ can be seen as an extension and a further refinement of the classical homogenization ansatz, in which only $\delta_1 \to 0$ holds.

While earlier theories were mostly interested in fully homogenized solutions as such, we investigated the possible contributions of first-order correc-

tions with respect to δ_1 and δ_2 to the numerically observed fluctuations. An important result, that manifests itself partially in formulas (22) and (23), states that the contribution of these first-order corrections to the local fluctuations are in most situations negligible as long as $\delta_1, \delta_2 \ll 1$. The circumstances under which the corrections become important can also be studied theoretically in our framework. As the main finding, we could show that the evolution of the fluctuation profile does not depend significantly on details of mass and electric transport in electrolyte, as e.g diffusion coefficient, etc. This theoretical conjecture was supported by the numerical comparison between microscopic model simulations of electrodes with graphite-like parameters and artificial one particle-system mimicking an absolutely homogeneous electrolyte with constant electric potentials in both phases.

After having thus estimated the role of non-homogeneity of the electrolyte and of the electric field in the cell state evolution in general and of their contribution to the fluctuations around averaged homogenized fields, we analyzed in more detail the zeroth-order solution, which is built as a sum of the solutions of independent particles. The fluctuations that one obtains from there depend only on non-isotropic properties of the individual particles (like non-spherical shape), one of the main factors missing in previous upscaling procedures. To obtain further analytical results, the relation between reaction currents and lithium concentration in the active material (equation (14), boundary conditions) was linearized. The resulting simplified mathematical analysis allowed us to identify the main parameters of charge-discharge dynamics that define the scale of fluctuations: average reaction current and slope of the dependence of exchange current on lithium concentration. Using

asymptotic analysis together with numerical experiments, we could identify quantitative trends between the size of local fluctuations and these parameters.

As the main conclusion of our mathematical upscaling procedure from microscopic model to DFN model, we find that the anisotropy-related interface variations of lithium concentration (and of the quantities that directly depend on it, like OCV, overpotential) do not disappear in the limit of full homogenization and small particle contact ($\delta_1 = 0, \delta_2 = 0$), and we do not see any rigorous procedure based on realistic assumptions about cell dynamics to eliminate these variations to make basic DFN model an exact homogenization limit of microstructure-resolving cell models. To extend computationally effective and intuitive DFN to incorporate processes and phenomena in which the localized fluctuations play a significant role, one has to utilize additional heuristic or rigorous mathematical arguments, which is part of ongoing research.

Acknowledgments

This work was funded by the Deutsche Forschungsgemeinschaft(German Research Foundation, DFG) in the framework of the research training group SiMET—Simulation of Mechanical, Electrical and Thermal Effects in Li-ion Batteries (281041241/GRK 2218).

References

[1] A. A. Franco, Multiscale modelling and numerical simulation of rechargeable lithium ion batteries: concepts, methods and challenges, RSC

Advances 3 (2013) 13027–13058. doi:10.1039/c3ra23502e.

[2] A. Latz, J. Zausch, Multiscale modeling of lithium ion batteries : thermal aspects, Beilstein Journal of Nanotechnology 6 (2015) 987–1007. doi:10.3762/bjnano.6.102.

[3] J. Newman, W. Tiedemann, Porous-electrode theory with battery applications, AIChE Journal 21 (1) (1975) 25–41. doi:10.1002/aic.690210103.

[4] M. Doyle, T. F. Fuller, J. Newman, Modeling of galvanostatic charge and discharge of the lithium/polymer/insertion cell, Journal of the Electrochemical Society 140 (6) (1993) 1526–1533. doi:10.1149/1.2221597.

[5] T. F. Fuller, M. Doyle, J. Newman, Simulation and optimization of the dual lithium ion insertion cell, Journal of the Electrochemical Society 141 (1994) 1–10. doi:10.1149/1.2054684.

[6] M. Doyle, J. Newman, The use of mathematical Modeling in the Design of Lithium/Polymer Battery Systems, Electrochimica Acta 40 (13) (1995) 2191–2196. doi:10.1016/0013-4686(95)00162-8.

[7] M. Doyle, J. Newman, A. S. Gozdz, C. N. Schmutz, J. M. Tarascon, Comparison of modeling predictions with experimental data from plastic lithium ion cells, Journal of the Electrochemical Society 143 (1996) 1890–1903. doi:10.1149/1.1836921.

[8] D. Bernardi, E. Pawlikowski, J. Newman, A general energy balance for battery systems, Journal of the Electrochemical Society 132 (1985) 5–12. doi:10.1149/1.2113792.

[9] C. R. Pals, J. Newman, Thermal modeling of the lithium/polymer battery ion discharge behavior of a single cell, Journal of the Electrochemical Society 142 (1995) 3274–3281. doi:10.1149/1.2049974.

[10] C. R. Pals, J. Newman, Thermal modeling of the lithium/polymer battery. II. Temperature profiles in a cell stack, J. Electrochem. Soc. 142 (1995) 3282–3288.

[11] W. B. Gu, C. Y. Wang, Thermal-electrochemical modeling of battery systems, Journal of the Electrochemical Society 147 (2000) 2910–2922.

[12] P. Arora, M. Doyle, R. E. White, Mathematical modeling of the lithium deposition overcharge reaction in lithium-ion batteries using carbon-based negative electrodes, Journal of the Electrochemical Society 146 (10) (1999) 3543–3553. doi:10.1149/1.1392512.

[13] C. Monroe, J. Newman, Dendrite growth in lithium/polymer systems, Journal of The Electrochemical Society 150 (10) (2003) A1377. doi:10.1149/1.1606686.

[14] J. Christensen, J. Newman, A mathematical model of stress generation and fracture in lithium manganese oxide, Journal of The Electrochemical Society 153 (6) (2006) A1019–A1030. doi:10.1149/1.2185287.

[15] V. Srinivasan, J. Newman, Discharge model for the lithium iron-phosphate electrode, Journal of The Electrochemical Society 151 (10) (2004) A1517–A1529. doi:10.1149/1.1785012.

[16] P. D. Vidtst, R. E. White, Governing equations for transport in porous

electrodes, Journal of the Electrochemical Society 144 (4) (1997) 1343–1353. doi:10.1149/1.1837595.

[17] C. Y. Wang, W. B. Gu, B. Y. Liaw, Micro-macroscopic coupled modeling of batteries and fuel cells. {I.} Model development, Journal of the Electrochemical Society 145 (1998) 3407–3417. doi:10.1149/1.1838820.

[18] W. Lai, F. Ciucci, Mathematical modeling of porous battery electrodes—Revisit of Newman's model, Electrochimica Acta 56 (11) (2011) 4369–4377. doi:10.1016/j.electacta.2011.01.012.

[19] F. Ciucci, W. Lai, Derivation of Micro/Macro Lithium Battery Models from Homogenization, Transport in Porous Media 88 (2) (2011) 249–270. doi:10.1007/s11242-011-9738-5.

[20] V. Taralova, Upscaling approaches for nonlinear processes in lithium-ion batteries, Ph.D. thesis, Technische Universität Kaiserslautern (2015). URL `http://nbn-resolving.de/urn:nbn:de:hbz:386-kluedo-40860`

[21] A. Latz, J. Zausch, Thermodynamic consistent transport theory of Li-ion batteries, Journal of Power Sources 196 (6) (2011) 3296–3302. doi:10.1016/j.jpowsour.2010.11.088.

[22] A. Latz, J. Zausch, Thermodynamic derivation of a Butler–Volmer model for intercalation in Li-ion batteries, Electrochimica Acta 110 (2013) 358–362. doi:10.1016/j.electacta.2013.06.043.

[23] M. Ender, An extended homogenized porous electrode model for lithium-ioncell electrodes, Journal of Power Sources 282 (2015) 572–580. doi:10.1016/j.jpowsour.2015.02.098.

[24] BEST – battery and electrochemistry simulation tool, https://www.itwm.fraunhofer.de/en/departments/sms/products-services/best-battery-electrochemistry-simulation-tool.html.

Table 1: Parameter set used in the microstructure simulation

Parameters/units	Value
$c_s^{(initial)}/mol/cm^3$	$2.639 \cdot 10^{-3}$
$c_s^{(max)}/mol/cm^3$	$2.4681 \cdot 10^{-2}$
$D_s/cm^2 s^{-1}$	10^{-10}
$\sigma_s/S/cm$	1.0
$\sigma^{(additive)}/S/cm$	10.0
$c_e^{(initial)}/mol/cm^3$	$1.2 \cdot 10^{-3}$
$t_+/1$	0.39989
$k_e/S/cm$	0.02
$D_e/cm^2 s^{-1}$	$1.622 \cdot 10^{-6}$
Current density,A/cm^2	$2.4 \cdot 10^{-3}$
$i_{00}/A/cm^{2.5} mol^{-1.5}$	0.002

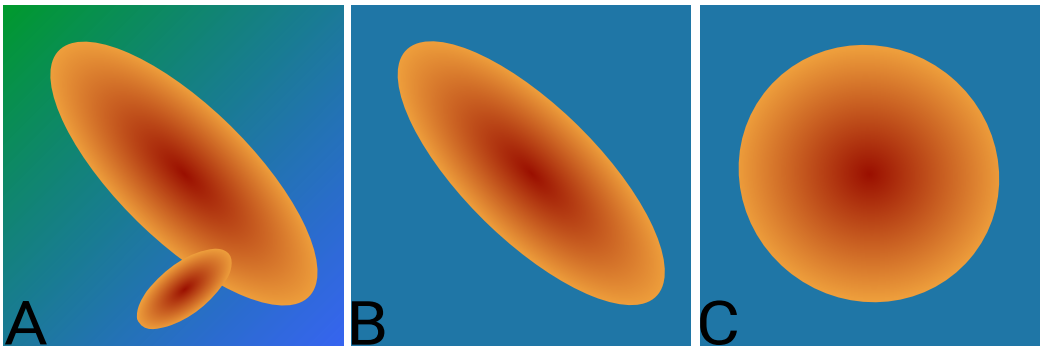

Figure 1: Schematic representation of different porous electrode models. Colors denote Li distribution. Subfigure A represents the microscopic model (1, 2), with local concentration and potential gradients allowed everywhere, and particle connections possible. Subfigure B is the eDFN model. Subfigure C is the electrode representation in the Newman model, with effective spherical particle

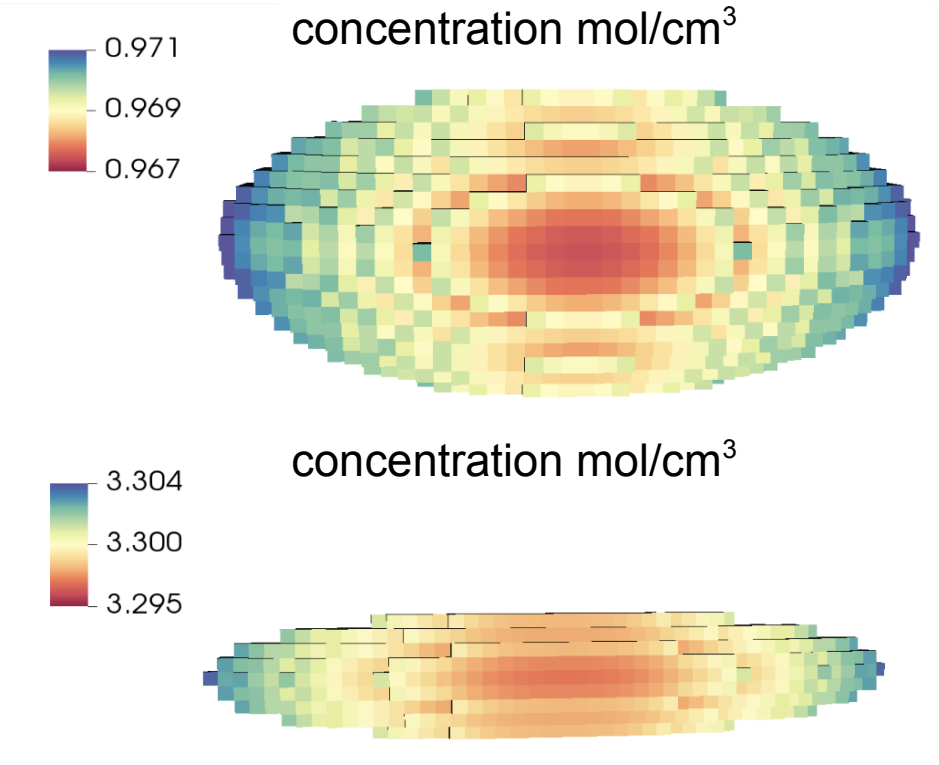

Figure 2: Concentration profiles for eDFN model. $\rho = 10$ for both particles, the particle above corresponds to the case $\varepsilon = 0.5$, the one below - to the case $\varepsilon = 0.2$.

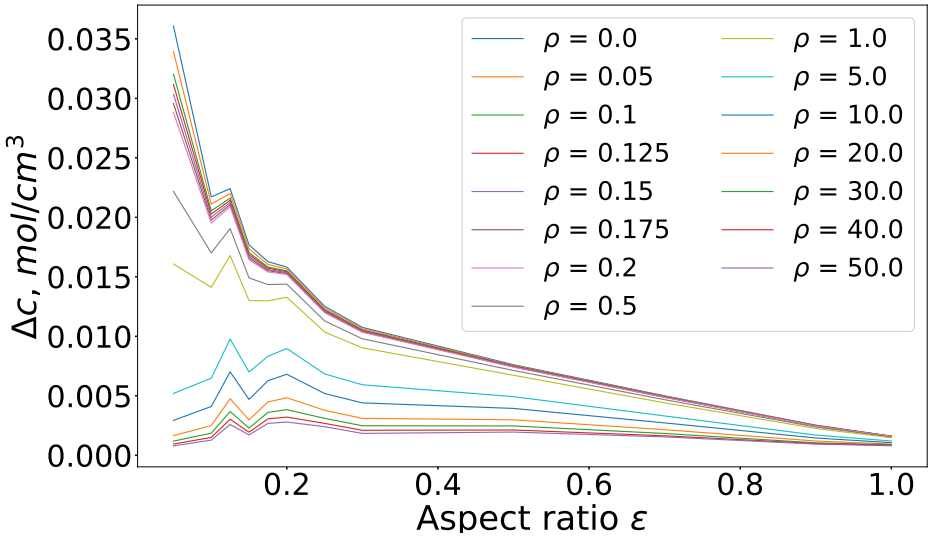

Figure 3: Total variation (maximum minus minimum) of the surface concentration as a function of the spheroid aspect ratio ε for different values of parameter ρ (see the text).

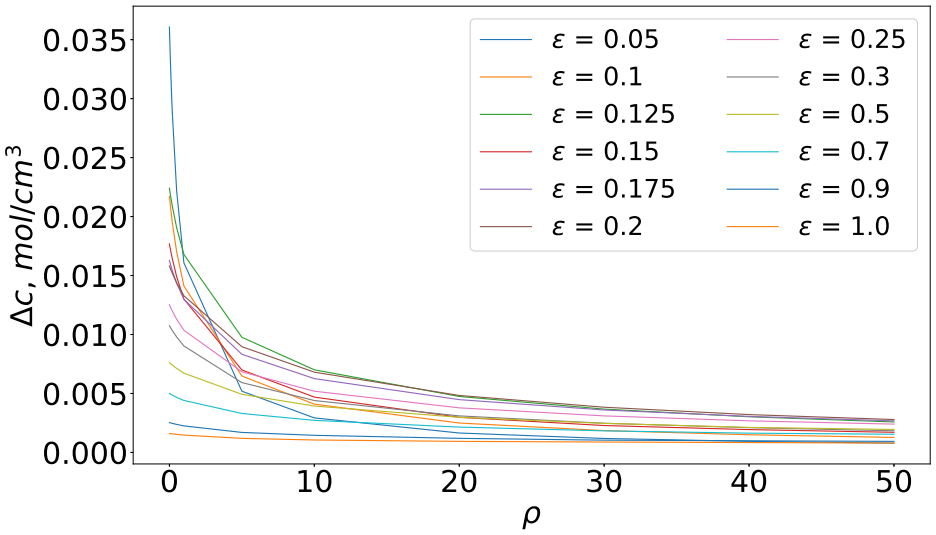

Figure 4: Total variation (maximum minus minimum) of the surface concentration as a function of ρ (see the text, proportional to the slope of the current reaction vs c_s) for different spheroid particle geometries (aspect ratio ε).

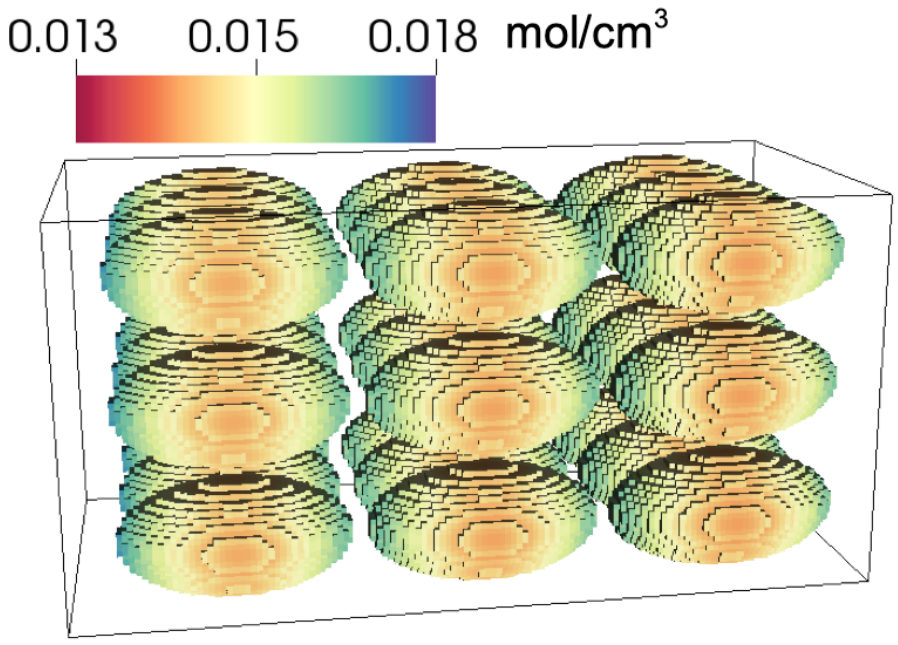

Figure 5: Lithium spatial distribution in the electrodes in the basic microscopic theory based simulation.

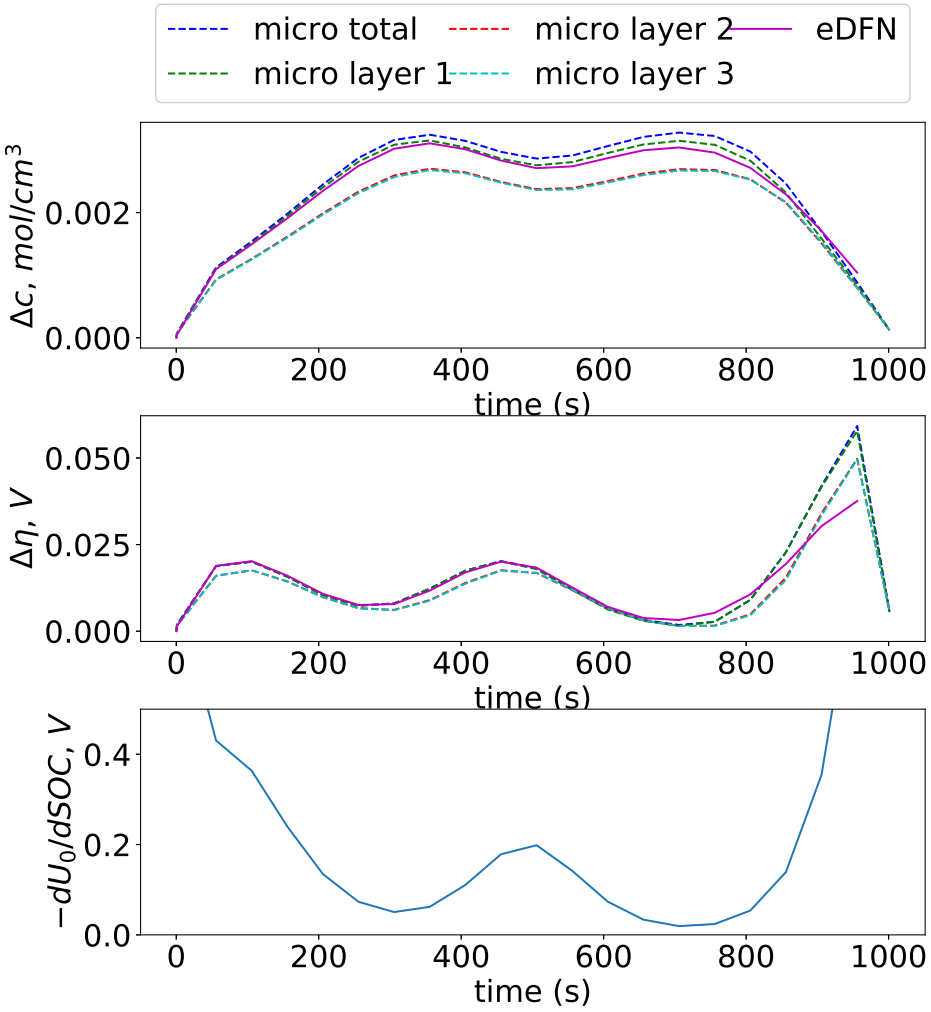

Figure 6: Evolution of the total variation (maximum minus minimum) of the concentration Δc and the overpotential $\Delta\eta$. The basic microscopic theory based simulation is compared to the eDFN simulation (the first refence system in the text). For the former, the results for separate electrode layers (defined in the text) are plotted too. The evolution of the OCV slope calculated at the surface-averaged values of concentrations and potentials is plotted below.

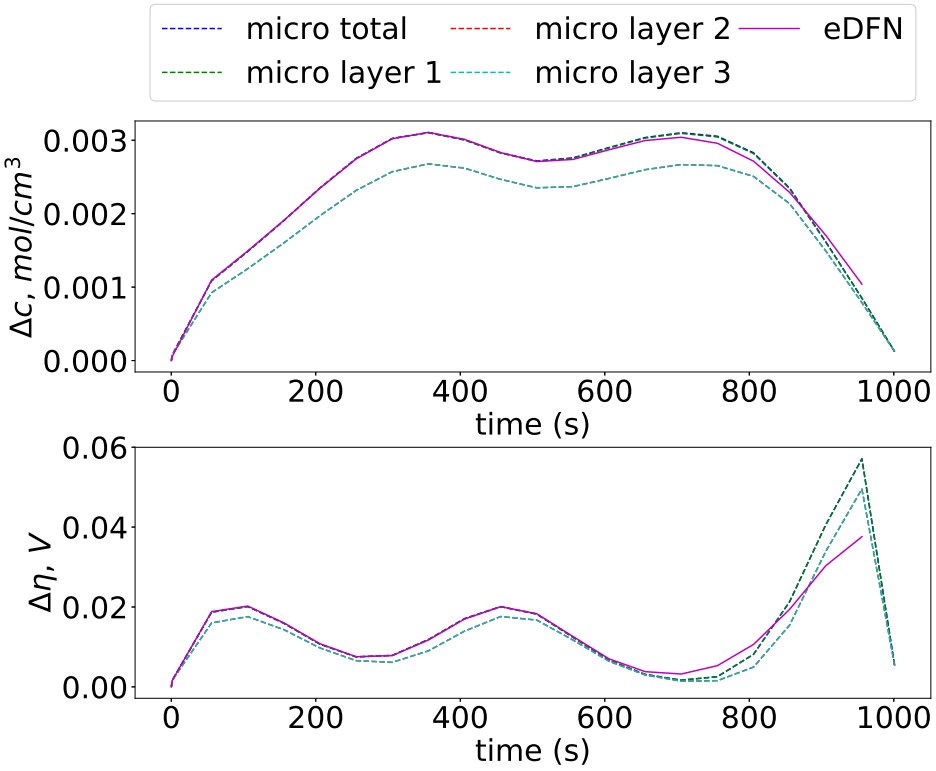

Figure 7: Evolution of the quantities from figure 6 when the basic microscopic theory based simulation is substituted with the one with all transport pararmeters multiplied by 100 (the second reference system in the text).

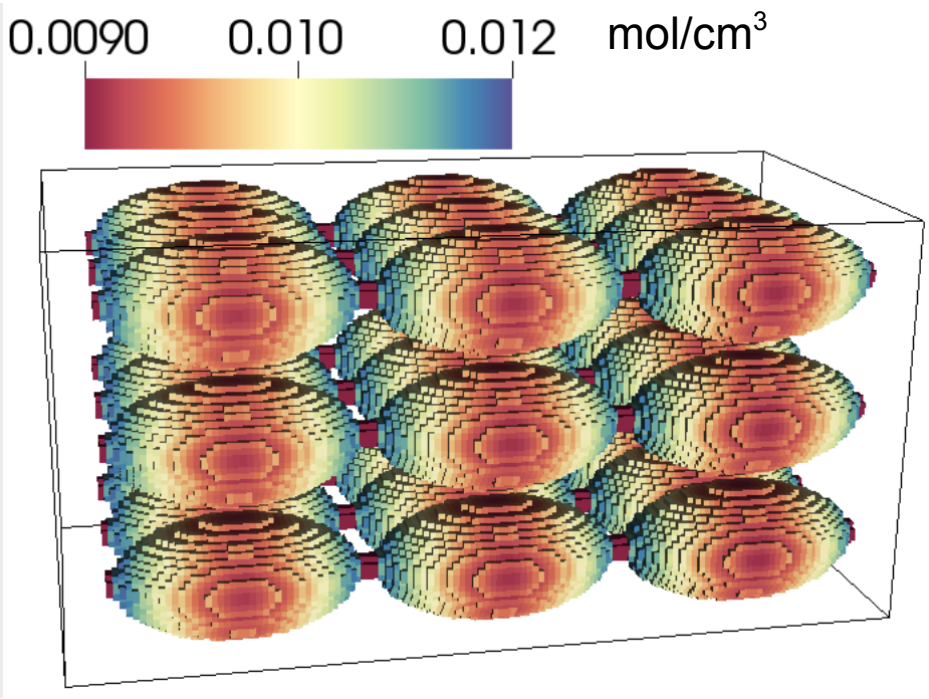

Figure 8: A snapshot of the lithium concentration evolution in the third reference system from the text, with dark red control volumes added, that represent the conductive material. To the right are 9 small conductive material plugs that differentiate this system from the basic one.

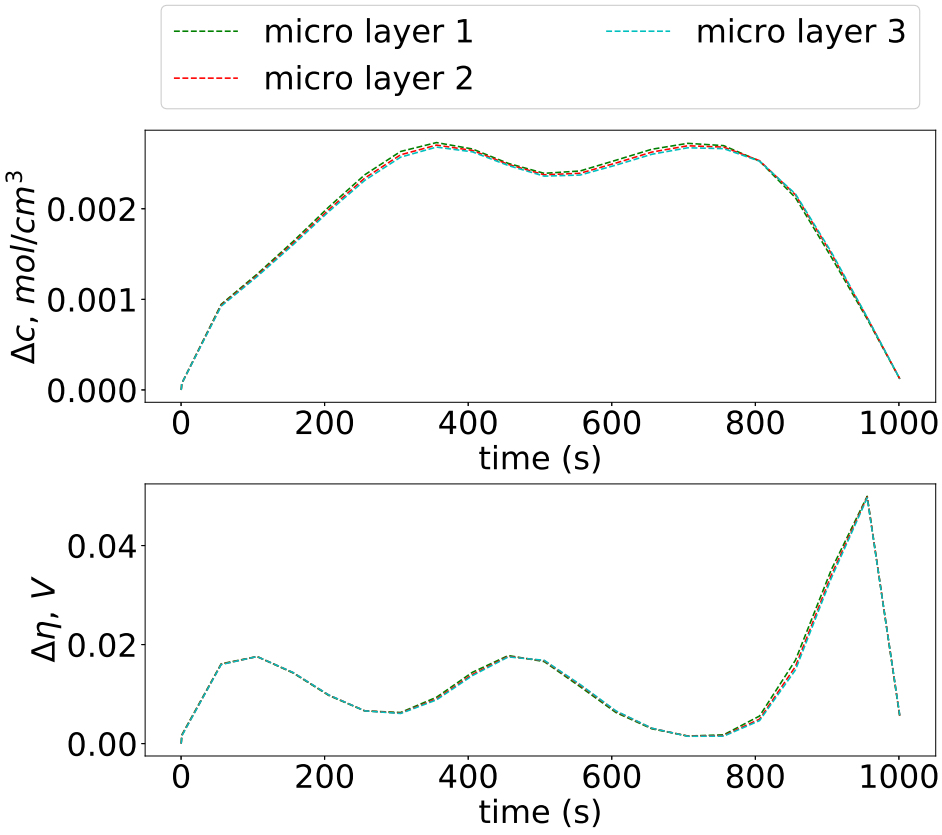

Figure 9: Evolution of the total variation (maximum minus minimum) of the concentration Δc and the overpotential $\Delta\eta$ in the second reference system from the text. The results for separate electrode layers (defined in the text) are plotted.

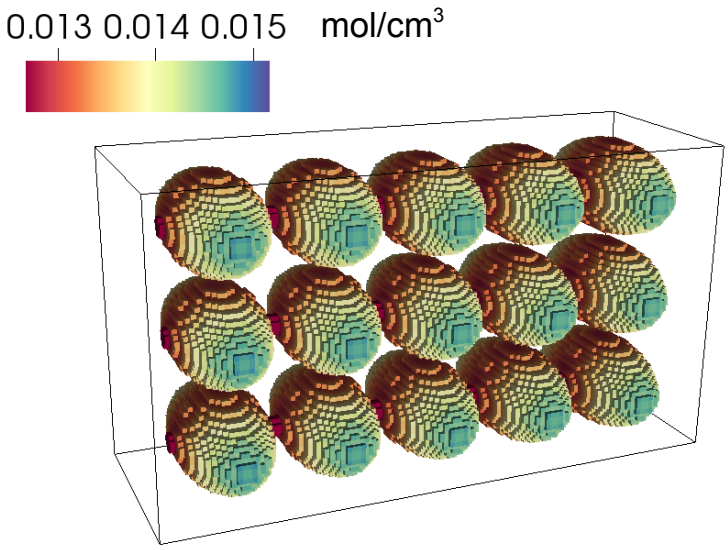

Figure 10: A snapshot of the lithium concentration evolution in the fourth reference system from the text, with dark red control volumes added, that represent the conductive material. The particle orientation is different from the other electrodes considered in the text.

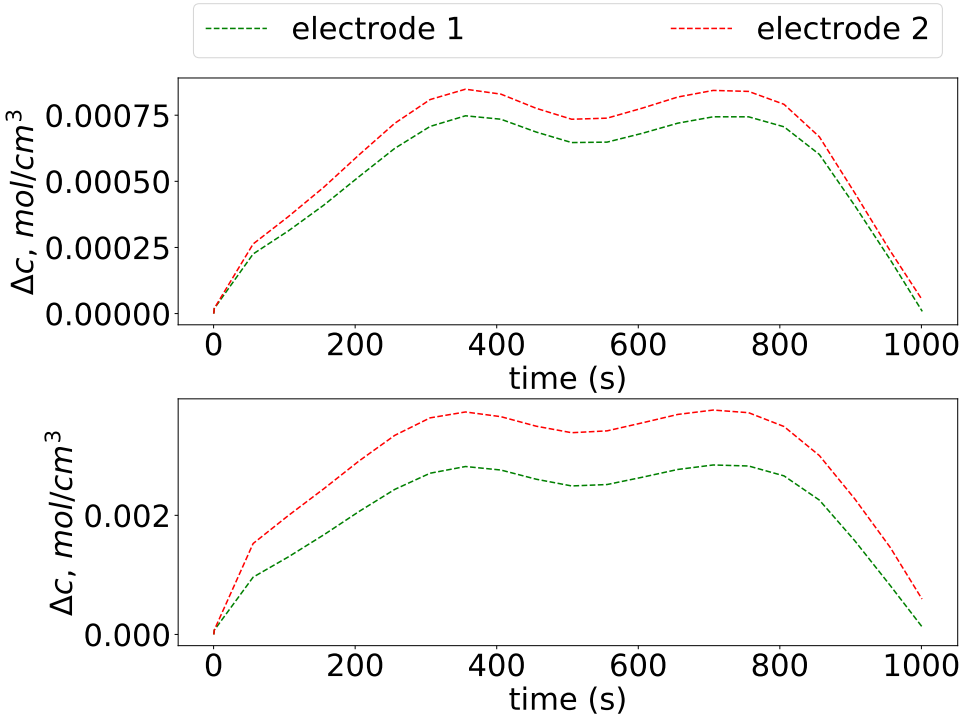

Figure 11: Evolution of the standard surface deviation (above) and the total variation (below) of the concentration c_s for the reference electrode systems from figure 8 (electrode 1) and figure 10 (electrode 2). The current density in the electrode 2 simulation is modified to keep the C-rates of both cases the same.

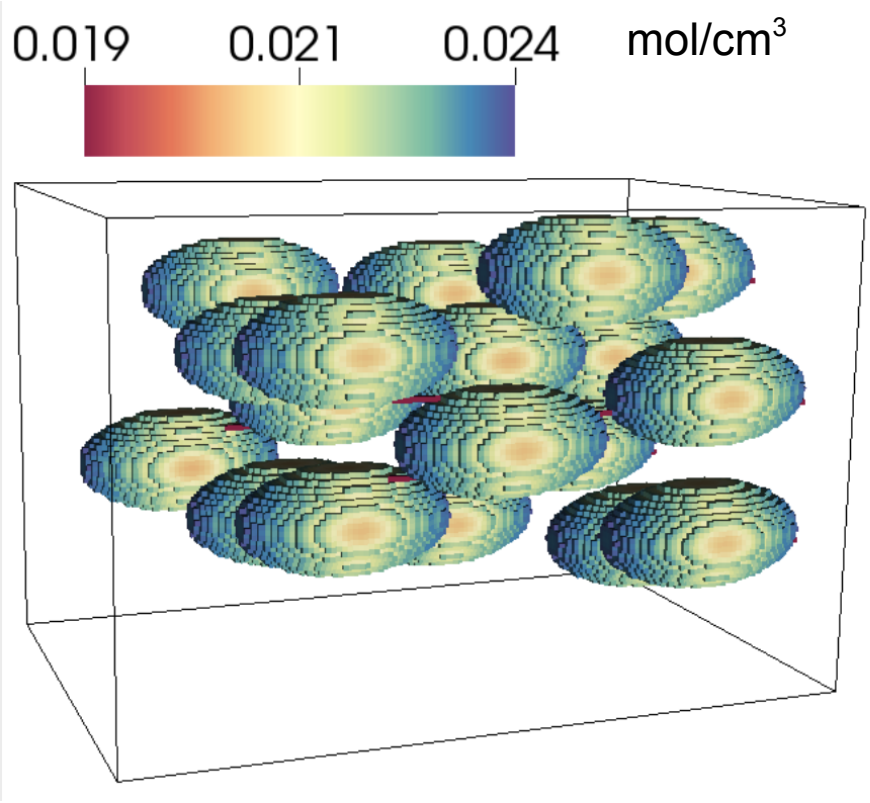

Figure 12: A snapshot of the lithium concentration evolution in the electrode microstructure built of the randomly located particles of strictly same geometrical shape. Dark red control volumes added, that represent the conductive material ensuring electric connectivity.

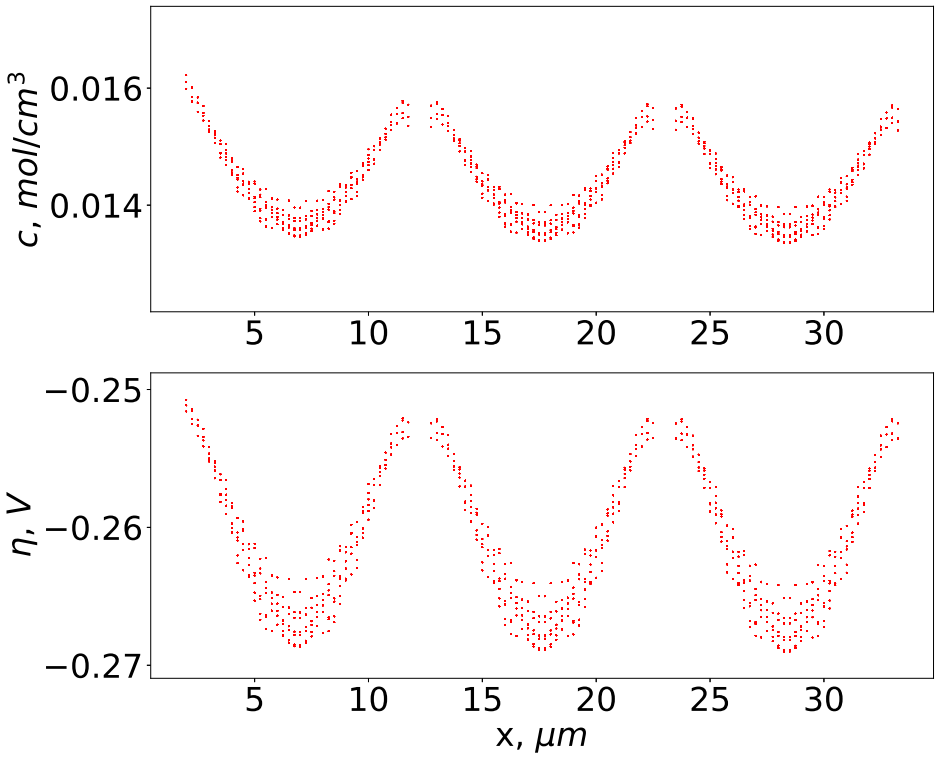

Figure 13: Projections of the concentration c and the overpotential η fields on the particle interfaces in the middle of the charging process for the electrode in figure 5.

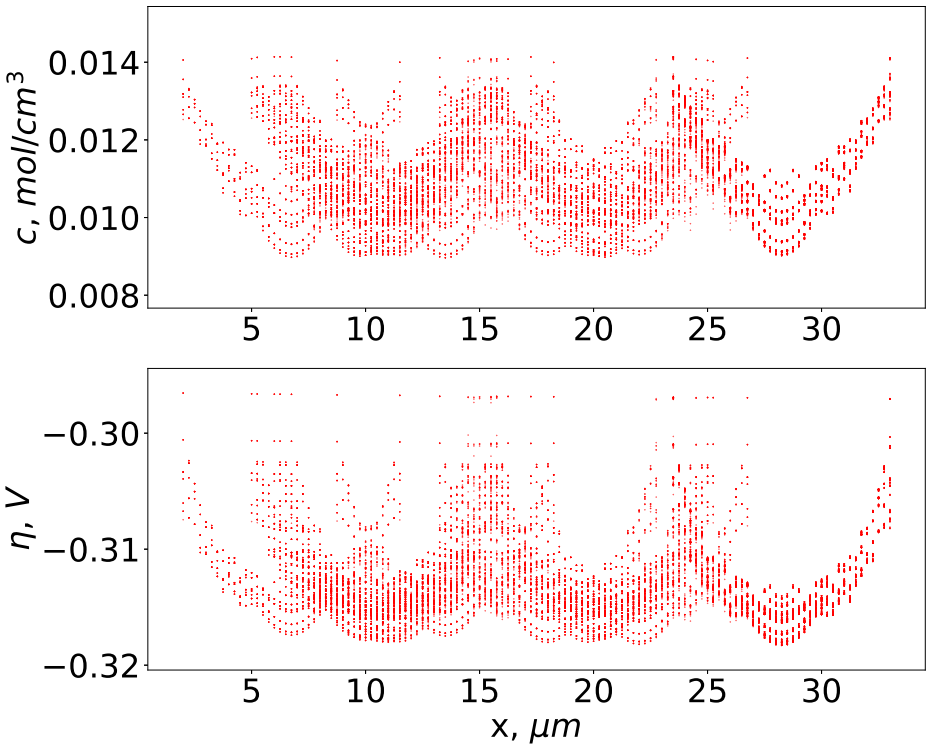

Figure 14: Projections of the concentration c and the overpotential η fields on the particle interfaces in the middle of the charging process for the electrode in figure 12.